Journal of Virology®

VACCINES AND ANTIVIRAL AGENTS

Autologous Antibody Responses to an HIV Envelope Glycan Hole Are Not Easily Broadened in Rabbits

Yuhe R. Yang,[a,b,c] Laura E. McCoy,[d] Marit J. van Gils,[e] Raiees Andrabi,[b,c,f] Hannah L. Turner,[a,b,c] Meng Yuan,[a,b,c] Christopher A. Cottrell,[a,b,c] Gabriel Ozorowski,[a,b,c] James Voss,[b,c,f] Matthias Pauthner,[b,c,f] Thomas M. Polveroni,[a,b,c] Terrence Messmer,[b,c,f] Ian A. Wilson,[a,b,c,g] Rogier W. Sanders,[e,h] Dennis R. Burton,[b,c,f] Andrew B. Ward[a,b,c,i]

[a]Department of Integrative Structural and Computational Biology, The Scripps Research Institute, La Jolla, California, USA
[b]Scripps Consortium for HIV/AIDS Vaccine Development (CHAVD), The Scripps Research Institute, La Jolla, California, USA
[c]IAVI Neutralizing Antibody Center and the Collaboration for AIDS Vaccine Discovery (CAVD), The Scripps Research Institute, La Jolla, California, USA
[d]Division of Infection and Immunity, University College London, London, United Kingdom
[e]Department of Medical Microbiology, Amsterdam UMC, University of Amsterdam, Amsterdam, the Netherlands
[f]Department of Immunology and Microbiology, The Scripps Research Institute, La Jolla, California, USA
[g]Skaggs Institute for Chemical Biology, The Scripps Research Institute, La Jolla, California, USA
[h]Department of Microbiology and Immunology, Weill Medical College of Cornell University, New York, New York, USA
[i]Ragon Institute of Massachusetts General Hospital, Massachusetts Institute of Technology, and Harvard University, Cambridge, Massachusetts, USA

Yuhe R. Yang and Laura E. McCoy contributed equally. Yuhe R. Yang was designated first author due to the structural focus of the manuscript, as she conducted the structural studies. Additionally, she took the lead in writing the manuscript, drafting figures, and revising the text. Laura E. McCoy undertook the antibody isolation and characterization as well as a substantial portion of the drafting of the manuscript.

ABSTRACT Extensive studies with subtype A BG505-derived HIV envelope glycoprotein (Env) immunogens have revealed that the dominant autologous neutralizing epitope in rabbits is located in an exposed region of the heavily glycosylated trimer that lacks potential N-linked glycosylation sites at positions 230, 241, and 289. The Env derived from B41, a subtype B virus, shares a glycan hole centered on positions 230 and 289. To test whether broader neutralization to the common glycan hole can be achieved, we immunized rabbits with B41 SOSIP (gp120-gp41 disulfide [SOS] with an isoleucine-to-proline mutation [IP] in gp41) alone, as well as B41 and BG505 coimmunization. We isolated autologous neutralizing antibodies (nAbs) and described their structure in complex with the B41 Env. Our data suggest that distinct autologous nAb lineages are induced by BG505 and B41 immunogens, even when both were administered together. In contrast to previously described BG505 glycan hole antibodies, the B41-specific nAbs accommodate the >97% conserved N241 glycan, which is present in B41. Single-particle cryo-electron microscopy studies confirmed that B41- and BG505-specific nAbs bind to overlapping glycan hole epitopes. We then used our high-resolution data to guide mutations in the BG505 glycan hole epitope in an attempt to broaden the reactivity of a B41-specific nAb, but we recovered only partial binding. Our data demonstrate that the lack of cross-reactivity in glycan hole antibodies is due to amino acid differences within the epitope, and our attempts to rationally design cross-reactive trimers resulted in only limited success. Thus, even for the immunodominant glycan hole shared between BG505 and B41, the prospect of designing prime-boost immunogens remains difficult.

IMPORTANCE A glycan hole is one of the most dominant autologous neutralizing epitopes targeted on BG505 and B41 SOSIP trimer-immunized rabbits. Our high-resolution cryo-electron microscopy (cryoEM) studies of B41 in complex with a B41-specific antibody complex elucidate the molecular basis of this strain-specific glycan hole response. We conclude that even for the immunodominant glycan hole shared between BG505 and B41, the prospect of designing prime-boost immunogens remains difficult.

Citation Yang YR, McCoy LE, van Gils MJ, Andrabi R, Turner HL, Yuan M, Cottrell CA, Ozorowski G, Voss J, Pauthner M, Polveroni TM, Messmer T, Wilson IA, Sanders RW, Burton DR, Ward AB. 2020. Autologous antibody responses to an HIV envelope glycan hole are not easily broadened in rabbits. J Virol 94:e01861-19. https://doi.org/10.1128/JVI.01861-19.

Editor Frank Kirchhoff, Ulm University Medical Center

Address correspondence to Dennis R. Burton, burton@scripps.edu, or Andrew B. Ward, andrew@scripps.edu.

Received 30 October 2019
Accepted 9 January 2020
Accepted manuscript posted online 15 January 2020
Published 17 March 2020

KEYWORDS HIV-1, SOSIP, autologous neutralization, epitope, glycan hole, monoclonal antibodies, rabbit immunization

With ~1.7 million new infections in 2018, human immunodeficiency virus (HIV) continues to be a major global public health issue (data from http://aidsinfo.unaids.org/). Although antiretroviral therapies (ARTs) have dramatically reduced mortality, preventative vaccines would be invaluable to control the spread of the pathogen. The human antibody response to HIV envelope glycoprotein (Env) following infection predominantly binds nonfusogenic conformations of Env, often referred to as "viral debris," as opposed to the intact fusogenic form displayed on the surface of the virus (1, 2). The corresponding antibodies are termed nonneutralizing and often recognize epitopes displayed both by conformationally open or partially disassembled Env and by glycoprotein 41 (gp41) subunit stumps, which remain after the glycoprotein 120 (gp120) subunit dissociates from the Env trimer. Infection can also elicit functional antibodies that bind the intact Env trimer and neutralize the virus strain prevalent in the infected host (3, 4). However, the virus can rapidly escape these strain-specific neutralizing antibodies (nAbs) by mutating the sequence within and proximal to the epitope and by adding glycosylation sites (5). In contrast, a small proportion of HIV-infected individuals develop broadly neutralizing antibodies (bnAbs), which recognize epitopes comprised of relatively conserved amino acids as well as N-linked glycans (6–8). These bnAbs are capable of neutralizing a high percentage of HIV strains. and their development has been associated with longer exposure to multiple evolving strains of the HIV (8). One approach to develop an effective vaccine capable of bnAb elicitation, therefore, involves cocktails of different trimer immunogens as well as sequential immunization with Envs derived from different strains (9, 10).

Antibodies elicited against stabilized HIV Env immunogen trimers (11, 12) can exhibit robust neutralization against immunogen-matched neutralization-resistant (tier 2) viruses in animal models. Our previous work in rabbits with immunogens derived from subtype A BG505 virus has revealed that an autologous neutralizing epitope region on BG505 is exposed and immunodominant due to the absence of glycan sites at position 241, which is present in >97% of HIV strains; at position 289, which is present in >70% of HIV strains; and at position 230, which is less conserved and present only in <35% of HIV strains (13–16). Certain other HIV strains lack some of the same glycan sites in the Env as BG505, resulting in partially overlapping holes in their glycan shield. These findings raised the question whether Env immunogens with overlapping glycan holes could be combined to induce broader tier 2 neutralizing responses. A stabilized and solubilized Env trimer (SOSIP; gp120-gp41 disulfide [SOS] with an isoleucine-to-proline mutation [IP] in gp41) derived from a subtype B Env gene, named B41, has been described previously (17) and has a partially overlapping glycan hole with that of BG505. Like BG505, B41 SOSIP lacks glycans at positions 289 and 230 but does contain the more highly conserved glycan at 241. Previous immunization studies with B41 SOSIP revealed that the majority of nAb responses in rabbits were indeed directed to the 289 glycan hole (17). However, the exact epitope and molecular details of the interactions with nAbs remain unknown.

In this study, we isolated B41-specific monoclonal Abs (mAbs) and confirmed that the dominant B41 autologous neutralizing response targets the 230/289 glycan hole on the B41 immunogen. Importantly, these nAbs can accommodate the highly conserved N241 glycan. Even when both BG505 and B41 immunogens were administered together, the isolated B41-specific nAb lineages were unable to cross-neutralize BG505, indicating no, or very limited, cross-boosting. We also show the molecular details of a B41-specific nAb bound to the 230/289 glycan hole epitope using high-resolution cryo-electron microscopy (cryoEM). Based on the amino acid contact residues between B41 and a B41-specific nAb, we then mutated BG505 to gain some binding of the B41 strain-specific nAb. In summary, we established that B41- and BG505-specific nAbs recognize different amino acids in their corresponding epitopes to block viral infection

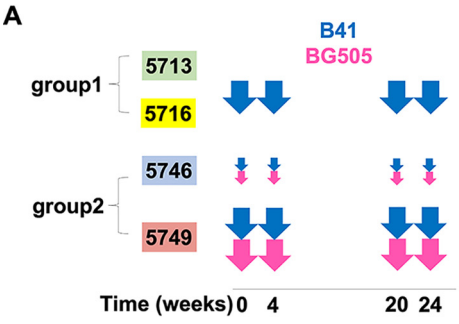

B

	B41	BG505
5713	704	NT
5716	700	NT
5746	3220	1800
5749	<50	768
C serum	<50	<50

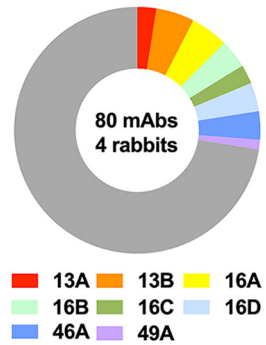

D

	mAb	B41	BG505
B41 SOSIP	13A	0.22	>50
	13A1	0.05	>50
	13B	0.30	>50
	13B1	0.07	>50
	13B2	1.49	>50
	13B3	0.55	>50
	16A	0.04	>50
	16A1	0.06	>50
	16A2	0.04	>50
	16A3	0.03	>50
	16B	0.78	>50
	16B1	0.13	>50
	16B2	0.02	>50
	16C	0.21	>50
	16C1	0.29	>50
	16D	10.37	>50
	16D1	0.03	>50
	16D2	5.33	>50

	mAb	B41	BG505
BG505 + B41 SOSIP	46A	0.20	>50
	46A1	0.13	>50
	46A2	0.05	>50
	49A	0.13	>50

FIG 1 Immunization schedule and autologous neutralizing activities of B41-specific rabbit mAbs. (A) Schematic of immunization schedule of four individual rabbits from two groups. Each immunization is indicated by an arrow, and every animal was immunized at the listed time points as described in Klasse et al. (14). Small and large arrows indicate different doses (10 μg or 30 μg per immunization). (B) Neutralization titers (ID_{50}) of immunized rabbit sera against B41 and BG505 pseudoviruses. Control (C) serum is from an unimmunized rabbit, 3421, described in the previous study (13). NT, not tested. (C) Pie chart showing that 22 of the 80 mAbs (28%) derived from four rabbits neutralize the immunogen-matched B41 pseudovirus (rabbit mAb families color-coded as in the legend below the pie chart). Nonneutralizing mAbs shown in gray. (D) Neutralization analysis of isolated nAbs against B41 and BG505 pseudoviruses. Inhibitory concentration (IC_{50}) values in μg/ml are listed.

and identified key residues that contribute to the antibody specificity. While our B cell isolation and antibody production were by no means exhaustive, given the prevalence of nAbs elicited against the shared glycan hole epitope in BG505 and B41, it is notable that no cross-nAbs were isolated. Interestingly, a large number of the nonneutralizing antibodies isolated were cross-reactive but likely bind to the irrelevant trimer base epitope. Therefore, we conclude that designing prime-boost or cocktail immunization regimens that increase the breath of glycan hole-directed nAb responses remains a challenge even with immunogens that share glycan holes.

RESULTS

B41 Env trimers induce autologous nAbs that do not cross-neutralize BG505. Four rabbits from a previously described immunization experiment (14) were used to isolate mAbs for the current study. In the prior study, animals were separated into the following two groups: group 1 (rabbits 5713 and 5716) received 30 μg B41 SOSIP trimer alone per immunization (large arrows), while group 2 (rabbits 5746 and 5749) received a bivalent cocktail containing both BG505 SOSIP and B41 SOSIP in a 1:1 ratio (10 μg or 30 μg per immunization, small and large arrows, respectively) (Fig. 1A). Group 1 animals 5713 and 5716, which only received the B41 immunogen, both had 50% infective dose (ID_{50}) neutralization titers against the wild-type B41 pseudovirus of around 1 in 700 (Fig. 1B), as expected given the single immunogen used. Of the two animals that received both immunogens, only 5746 had cross-neutralizing sera. Rabbit 5746, which received a low dose of the BG505/B41 cocktail, had a higher neutralizing titer (~3,300) against the wild-type B41 pseudovirus than BG505 pseudovirus (~1,800) (Fig. 1B). Rabbit 5749, which received a high dose of the BG505 SOSIP and B41 SOSIP cocktail, is BG505 specific and has an undetectable neutralizing titer against the wild-type B41 pseudovirus (Fig. 1B).

From these four animals, 80 mAbs that bound B41 SOSIP were isolated by single B cell sorting using both B41 and/or BG505 SOSIP as the bait and successfully PCR amplified (Fig. 1C). MAbs were named with a similar nomenclature as described previously (13). Each mAb was named according to the rabbit identifier (13, 16, 46, and 49 for rabbits 5713, 5716, 5746, and 5749, respectively) and then a unique alphabetical lineage identifier (e.g., A and B). Lineage members were then assigned with an additional number, for example, 13A1, 13B1, and 13B2. A total of 58 mAbs (72%) bound

A

	B41	B41 +kif	B41 N289	B41 N289 +kif	B41 N230	B41 N230 +kif	B41 N241-KO
13A	0.026	0.031	>50	3.801	0.034	0.062	0.806
13B	0.020	0.046	10.980	1.038	>50	>50	1.444
16A	0.010	0.004	>50	0.500	0.019	0.030	0.141
16B	0.035	0.010	>50	1.392	0.048	0.048	5.684
16C	0.016	0.007	>50	0.548	0.021	0.022	1.137
16D	0.806	0.309	>50	18.520	0.882	0.949	8.430
46A	0.021	0.034	>50	1.450	0.020	0.052	0.768
49A	0.128	0.597	>50	11.750	>50	>50	1.483
45A	>50	>50	>50	>50	>50	>50	>50

C

	B41	B41 +kif	B41 N289	B41 N289 +kif	B41 N230	B41 N230 +kif
5713	704	616	161	363	358	213
5716	700	502	<50	251	505	270
5746	3220	4254	<50	2584	1983	1299
5749	<50	70	<50	65	<50	<50
C serum	<50	<50	<50	<50	<50	<50

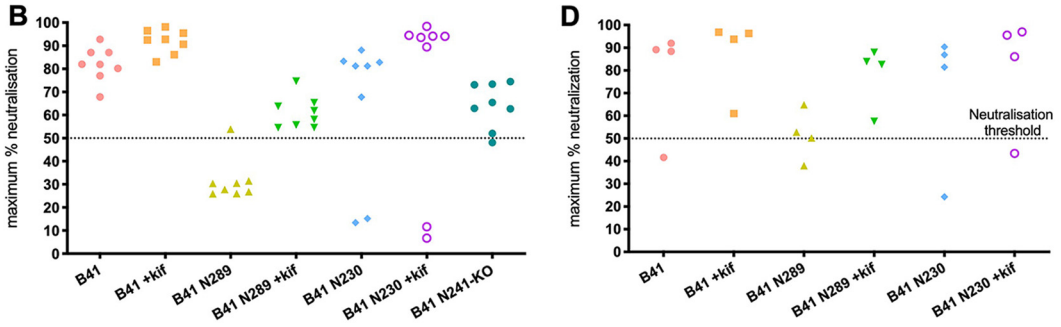

FIG 2 B41-specific rabbit nAbs target the 230/289 glycan hole. (A) Neutralization analysis of isolated nAbs against a panel of B41 mutants covering glycans at sites 230, 289, and 241. +kif indicates that the pseudovirus was grown in the presence of kifunensine. Inhibitory concentration (IC_{50}) values are listed in μg/ml. Non-nAb 45A was used as a control. The highest concentration tested for neutralization was 50 μg/ml. (B) Maximum neutralization percentage of isolated mAbs against autologous B41 virus and mutants. Maximum neutralization of mAbs was defined at 50 μg/ml. (C) Neutralization titers (ID_{50}) of immunized rabbit sera determined using B41 mutants. C serum is from an unimmunized rabbit 3421 as a control. NT, not tested. (D) Maximum neutralization percentage of sera against autologous B41 virus and mutants. The *y* axis shows the max neutralization percentage for sera from individual rabbits.

both BG505 and B41 immunogens but were unable to neutralize either BG505 or B41 pseudoviruses. Although these mAbs were not studied further, we suspect that the majority of them target the immunodominant epitope present on the soluble SOSIP trimer but not the viral surface membrane-embedded trimer (18). In contrast, 22 mAbs (28%) bound only the B41 immunogen. These mAbs derived from eight genetically distinct families, and all family members were able to neutralize the immunogen-matched B41 pseudovirus (Fig. 1C). The B41-specific nAbs exhibited strong neutralization against B41, with 50% inhibitory (IC_{50}) values as low as 0.02 μg/ml (Fig. 1D). Interestingly, none of these nAbs showed cross neutralization of BG505, even the mAbs from the 46A and 49A families isolated from the rabbits that received the BG505 and B41 SOSIP trimer cocktail. These data suggest that the BG505 and B41 immunogens induce independent autologous nAb responses.

B41-specific rabbit nAbs target the 230/289 glycan hole. Our previous work with BG505 immunogens in rabbits revealed that the dominant autologous nAbs target the glycan hole created by the absence of glycans at positions 230, 241, and 289 (13). Moreover, autologous neutralization specific for glycan holes was also seen following immunization with trimers from different clades (19). To determine whether the B41 nAbs also targeted a glycan hole on the B41 immunogen, we tested the neutralization activity of eight isolated mAbs representing the different autologous nAb families using a panel of B41 mutant pseudoviruses with the N230 and N289 glycans knocked in (Fig. 2A and B). Introduction of the N289 glycan abolished or greatly reduced the neutralization activity for all eight nAbs (Fig. 2A), which was reflected in a significant reduction of the maximum neutralization capacity (Fig. 2B). The detrimental effect of introducing the N289 glycan was largely mitigated when the pseudovirus was grown in the presence of kifunensine to enrich for oligomannose glycans (Fig. 2A and B), where the maximum neutralization values were increased above the 50% neutralization threshold, allowing the calculation of IC_{50} values. In contrast, neutralization activity for all nAbs was only mildly affected when the wild-type B41 pseudovirus was grown in the

presence of kifunensine. Furthermore, while introduction of the N230 glycan (with or without kifunensine) eliminated neutralization activity for nAbs 13B and 49A, it had no effect on the other six nAbs. The role of the N241 glycan was tested with B41 N241-knock out (KO) pseudovirus and showed that neutralization was in some cases diminished but not abolished entirely for any of the nAbs.

We then tested sera neutralization activity with the same panel of B41 mutant pseudoviruses to evaluate if the activity of individual nAbs is representative of the activity in the sera (Fig. 2C and D). Consistent with the observations made using the nAbs, the introduction of a glycan site at position 289 greatly decreased the neutralization activity in all 4 rabbit sera (Fig. 2C and D), suggesting that the isolated mAbs represent a substantial proportion of the nAbs within the sera. Moreover, the same restoration of neutralization activity was observed when the sera were tested against the N289-knock-in (KI) virus expressed in the presence of kifunensine. In addition, the introduction of a glycan site at position 230 had relatively little effect on serum neutralization.

B41-specific rabbit nAbs resemble BG505-specific glycan hole nAbs in a number of respects but do not neutralize BG505 virus. Enzyme-linked immunosorbent assay (ELISA) binding assays showed that all 8 nAbs bound to B41 SOSIP, while 6/8 also bound to B41 gp120 (Fig. 3A). nAbs 13B and 49A were not able to bind to B41 gp120 (Fig. 3A). Given the gp120-specific nature of their epitopes revealed by our structural studies (below), the most likely reason for not binding is a difference in the glycosylation pattern of gp120 versus the Env trimer. Non-nAbs 45A and 48A, which were isolated in parallel from a previous study (14), show strong binding to the B41 SOSIP trimer but not to gp120. Competition ELISAs using previously described bnAbs that target distinct epitopes were conducted to locate the epitopes of the B41 mAbs (Fig. 3B; see Fig. S5 in the supplemental material). PG9, PGT121, 8ANC195, and PGV04 that target the trimer apex, N332-glycan supersite, gp120-gp41 interface, and CD4-binding site epitopes, respectively, were used in the analysis (Fig. 3C). The results showed that 49A and 13B compete with the human gp120-gp41 interface specifically with bnAb 8ANC195, indicative of overlapping epitopes. The B41 nAbs also exhibited a high level of competition between themselves, suggesting that they targeted a common epitope (Fig. S5).

We next carried out single-particle negative-stain electron microscopy (NS-EM) to more precisely determine the location of the epitopes targeted by the isolated mAbs. Epitope mapping of 8 mAbs resulted in only 2 classes of epitopes (Fig. 3D to F). Class 1 contained the nonneutralizing base binders 45A and 48A that targeted the base of the B41 trimer at different angles (Fig. 3E; see Fig. S2 in the supplemental material). Representative two-dimensional (2D) classes showed that 48A binds with a stoichiometry of three antibodies per trimer, while 45A only binds with one to two antibodies per trimer. Class 2 included 6 nAbs targeting an overlapping epitope around the 230/289 glycan hole region, confirming the mutant neutralization and competition binding results. Representative 2D classes showed that all nAbs bind with a stoichiometry of three antibodies per trimer. Representative 3D EM reconstructions from B41-13B and B41-49A complexes were shown to further illustrate the epitope (Fig. 3F). The epitope overlaps considerably with the BG505-specific glycan hole antibody 11A, and the antibodies approach the trimer with similar upward angles (Fig. 3F).

NS-EM, ELISA, and neutralization data confirm that the B41-specific antibodies target a similar glycan hole region as the previously described BG505-specific mAbs 10A, 11A, and 11B (13). However, our neutralization results demonstrate that B41-isolated mAbs lack the ability to neutralize BG505 (Fig. 1D), including the 46A and 49A family nAbs that are elicited in rabbits immunized with the B41 and BG505 cocktail. To further understand why there was no cross-reactivity of neutralizing Abs targeting an overlapping glycan hole epitope, cryoEM structural studies were conducted on B41 SOSIP in complex with 13B. While 13B was isolated from a B41 SOSIP-only immunized animal, it was representative of all the B41-specific nAbs, as illustrated by the structural similarity revealed by NS-EM.

A

	EC_{50} µg/ml	
	SOSIP	gp120
13A	0.02	0.02
13B	0.03	>50
16A	0.03	0.01
16B	0.02	0.01
16C	0.03	0.02
16D	0.18	0.04
46A	0.02	0.02
49A	0.03	>50
blank	>50	>50
45A	0.06	>50
48A	0.17	>50
Hybrid	>50	>50

B

	Biotinylated-competitors			
	PG9	PGT121	8ANC195	PGV04
13A	122	107	70	99
13B	115	93	23	57
16A	182	115	85	98
16B	171	111	74	99
16C	178	112	78	102
16D	182	118	93	107
46A	178	117	75	108
49A	114	102	11	74
blank	112	98	98	100
45A	134	99	83	101
48A	72	81	79	90
Self	30	15	46	36

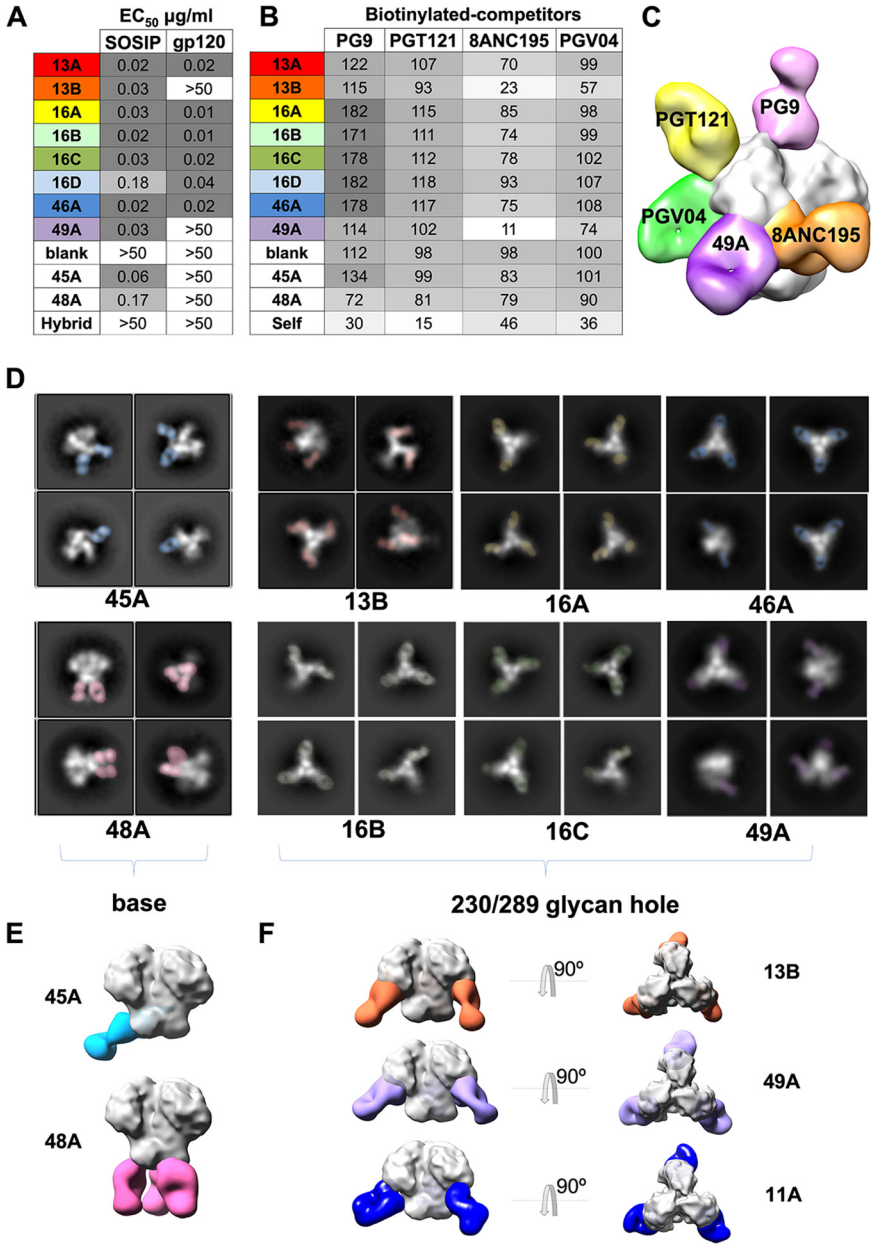

FIG 3 Epitope mapping by competition assay and negative-stain electron microscopy (NS-EM). (A) Enzyme-linked immunosorbent assay (ELISA) of isolated mAbs against the B41 gp120 monomer and B41 SOSIP trimer. The 50% effective concentrations (EC_{50}s) in μg/ml are listed. Non-nAbs (45A and 48A) were isolated in parallel with the antibodies described here. The negative-control mAb, named Hybrid, was made from the heavy chain of R56 and light chain of R20 (PDB 4JO3) used in a previous study (13). (B) Competition ELISAs of isolated mAbs against previously identified bnAbs. The percent binding of biotinylated bnAbs was tested in the presence of the indicated nonbiotinylated rabbit mAb competitors. The data represent the percentage reciprocal binding where 100% was the absorbance measured for each bnAb in the absence of any competitor. (C) Three-dimensional reconstruction comparison of the nAb 49A epitope to previously identified bnAbs. (D) Representative 2D classes (bottom) of different mAbs. (E) Representative 3D reconstructions of base binding antibodies, 45A (blue) and 48A (pink), and (F) glycan hole-targeting antibodies, including 13B (orange), 49A (purple), and 11A (dark blue) bound to B41 SOSIP.

A high-resolution cryoEM structure of 13B in complex with the B41 SOSIP trimer reveals atomic details of recognition. To characterize the binding mode of the B41-specific antibodies, we have obtained an ~3.9-Å resolution cryoEM map reconstruction of nAb 13B in complex with the B41 SOSIP trimers and built an atomic model

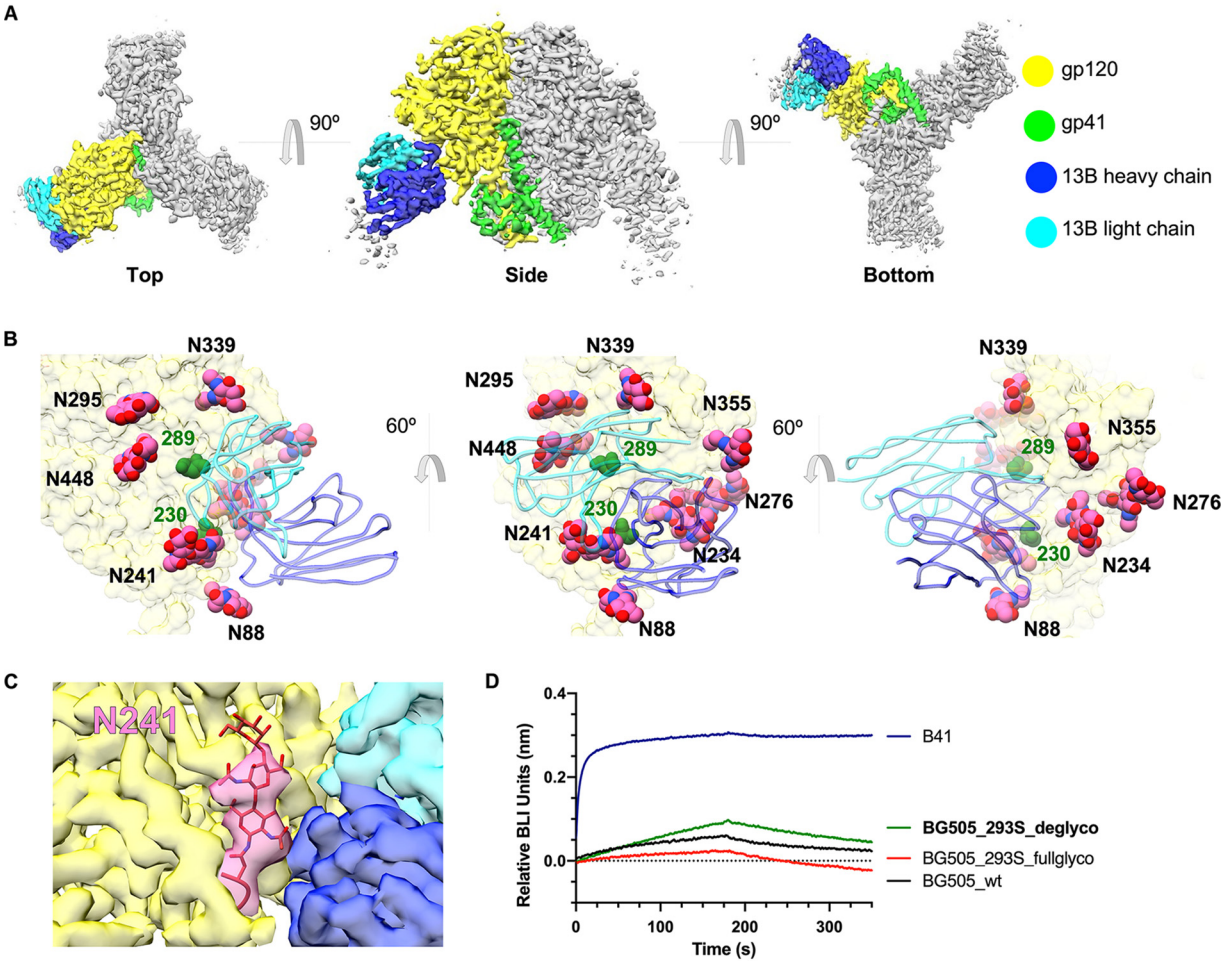

FIG 4 CryoEM map and model of B41-13B at 3.9 Å. (A) Top, side, and bottom view of a cryoEM 3D reconstruction of B41-13B complex at ~3.9-Å resolution colored by subunits. (B) Zoomed-in image showing how antibody 13B targets the 230/289 glycan hole epitope (230 and 289 residues highlighted in dark green); modeled glycans (spheres) in pink, ribbon representation of 13B Fab in blue (dark, heavy chain light, light chain), and B41 gp120 surface in yellow. (C) The density map shows that 13B (light and dark blue) interacts exclusively with gp120 peptide (yellow), and although the N241 glycan (highlighted in pink) is close by, no direct contacts are observed. When the previously solved crystal structure (PDB 6MCO) of B41 SOSIP was docked into our cryoEM density map, the N241 glycan (red sticks) fit exactly into the cryoEM density for the glycan. (D) Biolayer interferometry (BLI) binding sensorgrams showing association and dissociation of His-tagged B41 SOSIP (blue) and BG505 SOSIP variants with 13B Fab. Deglycosylated BG505 SOSIP is colored in green, HEK293S-expressed BG505_fullglyco without EndoH treatment in red, and HEK293F-expressed BG505_wt SOSIP in black.

(Fig. 4A). A starting model was created by combining a homology model of the Fv region of 13B generated using the Rosetta antibody protocol (20) and a B41 SOSIP crystal structure (PDB 6MCO). 13B binds to the glycan hole epitope with the heavy chain making the majority of contacts. This is different from the BG505 glycan hole nAbs which appear to interact primarily via the light chain (18). The glycan hole epitope is surrounded by 8 glycans, including N88, N234, N241, N276, N295, N339, N355, and N448 (Fig. 4B), which likely constrain the angle of approach for the elicited antibodies. The first two sugars of the N241 glycan (which is present in B41 but not BG505) were resolved in the refined map (Fig. 4C). The glycan density is in close proximity to the 13B density but remains distinct, indicating no direct contact. The identical conformation for the N241 glycan was observed in our B41-13B structure as well as a previously solved crystal structure of B41 (PDB 6MCO) that did not have a glycan hole antibody bound, indicating that the binding of 13B did not result in a conformational change of the glycan. These data are consistent with our conclusion that 13B does not specifically interact with the N241 glycan.

To further evaluate the role of glycans in antibody binding, a deglycosylated version of BG505 SOSIP was prepared by expression in HEK293S cells followed by EndoH

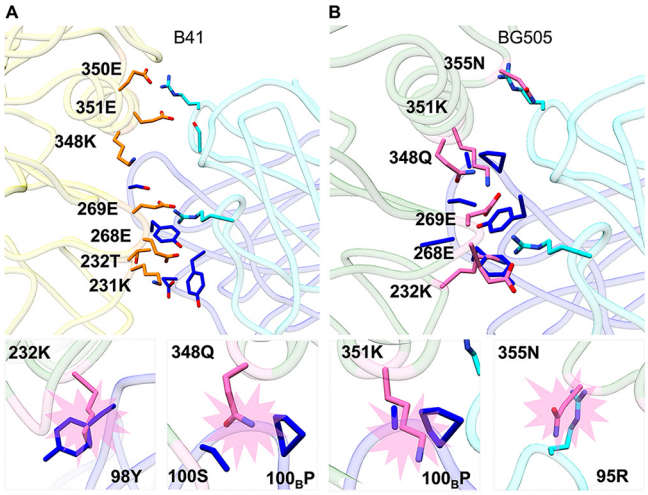

C

HXB2 numbering	231	232	268	269	348	350	351	355
B41	K	T	E	E	K	E	E	N
BG505	K	K	E	E	Q	R	K	N

FIG 5 Structural comparison of BG505 SOSIP and B41 SOSIP with B41-elicited rabbit antibody 13B bound to its epitope. (A) Contact residues at the B41-13B interface. Contact residues are defined as two residues containing any atom within 4 Å of each other; B41 residues are colored orange and 13B residues in light (light chain) and dark (heavy chain) blue. (B) Superimposition of BG505 (PDB 5CEZ) and B41-13B complex aligned on gp120. For clarity, the B41 trimer is not shown. Potential residues that clash between BG505 and 13B are highlighted in pink sticks. Below are zoomed-in structures of 4 potential clashes of BG505 with 13B involving 3 with the heavy chain (232K-98Y, 348Q-100_BP//100S, and 351K-100_BP) and 1 with the light chain (355N-95R). The heavy chain is in dark blue, BG505 potential clashing residues in pink, light chain residues in light blue, and gp120 of BG505 in light green. (C) Sequence alignment of potential contact residues of B41 (highlighted in orange) with 13B and potential clashing BG505 residues (highlighted in pink) modeled with 13B.

treatment (see Fig. S3A in the supplemental material). Biolayer interferometry (BLI) analysis against 13B was compared in parallel with positive-control B41, negative-control wild-type BG505, as well as HEK293S-expressed BG505 before EndoH treatment (Fig. 4D). The removal of glycans of BG505 only resulted in a subtle impact on binding to 13B, and differences in binding affinity could not be reliably calculated with the observed binding curves. When we further tested binding of 13B with deglycosylated BG505 by NS-EM, no complex formation was observed (Fig. S3B). These data support the conclusion that the lack of cross-reactivity to BG505 is, therefore, not due to glycan differences. Thus, we concluded that protein sequence differences between BG505 and B41 within the epitope region are responsible for the lack of cross-reactivity.

The high-resolution structure of B41 allowed a direct comparison of the epitope regions of B41-specific and BG505-elicited rabbit nAbs (13). To identify residues in B41 that contribute to binding, we highlighted all of the potential contact residues of B41 and 13B (Fig. 5A). The contact residues are defined as two residues containing any atom within 4 Å of each other, as determined using Chimera (21). Next, we superimposed the high-resolution BG505 model (PDB 5CEZ) on the gp120 subunit of B41 SOSIP to identify potential clashing residues, which we defined as atoms closer than 1.0 Å (Fig. 5B). The potential clashes involved three residues in the heavy chain, namely, Y98 (heavy chain) with K232 (Env), $P100_B$ and 100S with Q348, and $P100_B$ with K351, as well as one in the light chain, namely, R95 with N355. Four residues in the epitope regions differ between B41 and BG505, as shown in the sequence alignment (Fig. 5C). Interestingly, despite being identical in the two Envs, residues 268 and 269 clash in our BG505 docked model, indicating that neighboring residues that differ between the strains caused structural perturbations in these conserved residues.

Based on our structural analyses, we generated a series of mutant BG505 SOSIPs, including switching all BG505 clash residues, as well as nonclashing residues within the

A

mutation groups	mut1			mut2					mut3		N241 KI	
mutations on BG505	K229N	230S	K232T	R350E	K351E	H352Q	G354P	N356K	K347A	Q348K	P240T	S241N

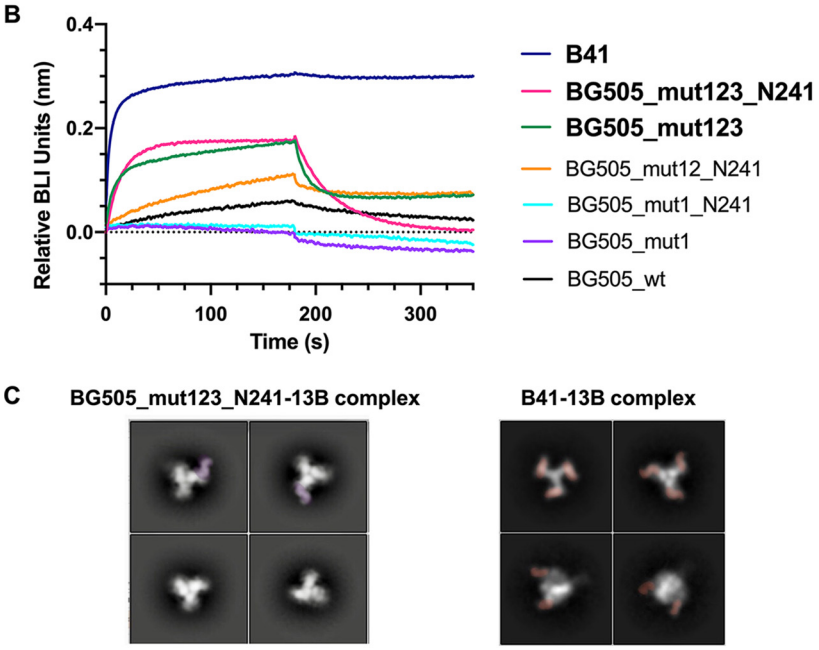

FIG 6 Restoration of binding of B41-specific antibody to BG505 mutants. (A) Mutations in the 4 different regions. (B) BLI binding analysis of B41 (dark blue) and a series of BG505 mutants (color codes shown on the right) against the 13B antibody. (C) Comparison of 2D classes between BG505_mut123_N241-13B complex (stoichiometry of zero to one antibody per BG505_mut123_N241 trimer) and B41-13B complex (stoichiometry of three antibodies per B41 trimer).

antibody binding footprint to B41 residues. We aimed to transfer B41-specific nAb binding properties to the BG505 trimer by generating the following changes: K232T, P240T, K347A, Q348K, and K351E. The K232T, Q348K, and K351E changes were included based on the above consideration that these should remove clashes with nAb 13B, while P240T and K347A were included to restore contact residues and recover binding. We note that some of the clashes may be indirect consequences of the presence of different neighboring amino acids that cause a rearrangement of the peptide backbone nearby, particularly the loops containing residues 231 to 232 and 268 to 269. Therefore, we expanded the mutations to 4 different regions, including 229 to 232 (mutation 1 [mut1]), 350 to 356 (mut2), 347 to 348 (mut3), and 240 to 241 (N241 knock-in), while retaining the rest of the residues (Fig. 6A).

BLI and NS-EM were used to screen the effect of different mutations in BG505 SOSIP on 13B binding. By combining 229 to 232 (mut1), 350 to 356 (mut2), 347 to 348 (mut3), and 240 to 241 (N241 knock-in) mutations (Fig. 6A), we partially conferred 13B binding capabilities on BG505 SOSIP. B41 SOSIP showed strong binding and no off-rate against 13B (dark blue), BG505_mut123_N241 and BG505_mut123 both exhibited binding with high off-rates against 13B, and all the other mutants exhibited similarly poor binding as 13B to BG505_wild type (wt) (Fig. 6B). To confirm BG505 mut123_N241 binding to 13B and obtain more structural insights into the complex, we incubated 10-fold excess Fab (molar ratio to trimer) with BG505_mut123_N241 overnight and conducted NS-EM studies. The 2D classes showed a stoichiometry of zero to one antibody per trimer (Fig. 6C). Among the particles collected, ~57% were trimers that had no Fab bound and ~43% of the particles had one Fab bound. No classes with more than one 13B antibody bound were found in 2D classifications even with 10-fold excess Fab. This

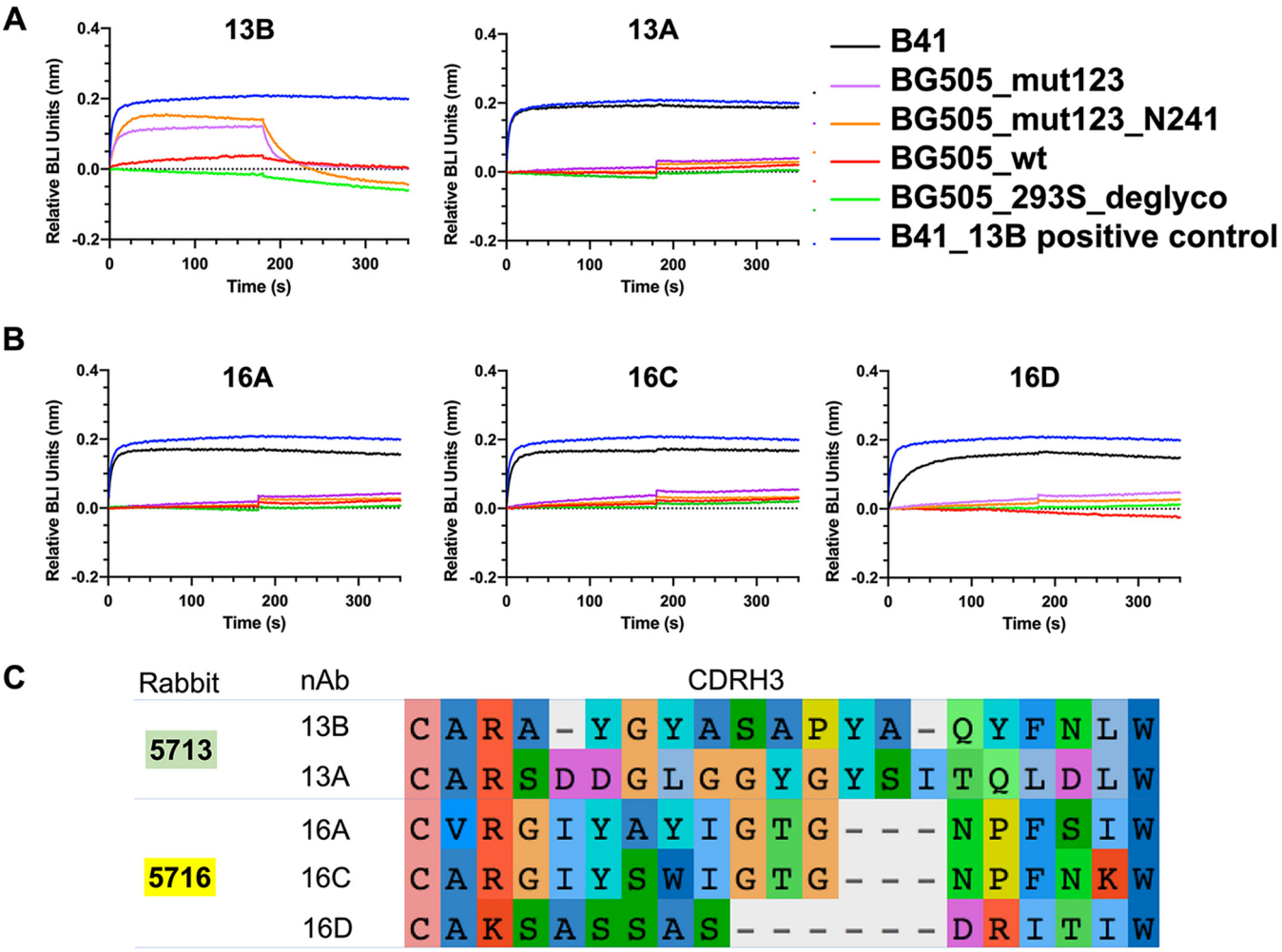

FIG 7 BLI analysis of B41 (black) and a series of BG505 mutants against rabbit antibodies, including 13B and 13A (A); 16A, 16C, and 16D (B); BG505_wt (red); BG505_deglyco (green); BG505_mut123 (purple); BG505_mut123_N241 (orange); and B41_13B (blue) as a positive control. (C) Sequence alignment of the CDRH3 of representative rabbit nAbs. Residues are colored with default settings in AliView (34).

result is consistent with weaker binding of BG505_mut123_N241 and 13B than B41 SOSIP with 13B.

To further assess the role of N241 in epitope recognition, we compared the BG505_mut123 with and without the N241 knock-in by both BLI and NS-EM analysis. The BLI results showed that, in the presence (Fig. 6B, pink) and absence (Fig. 6B, green) of the N241 glycan, BG505 bound 13B similarly. Although the sample lacking N241 results in slightly faster on and off rates, the overall trace is very similar, again confirming that N241 is not a crucial factor for accessing and binding to the epitope.

The NS-EM and BLI binding data both show that we enabled binding of BG505 mut123 and BG505 mut123_N241 to 13B. The relatively rapid on-rates to these mutants indicate that residues hindering the BG505 and 13B interaction have been removed. However, the high off-rate suggests that the complex is still not as stable as 13B in complex with B41 SOSIP, likely due to fewer productive interactions.

We generated some level of cross-reactivity with glycan hole-targeting antibody 13B by introducing B41 mutations to the glycan hole epitope region of BG505 (Fig. 6). Binding of B41 and BG505 mutants with four other B41-specific glycan hole nAbs was tested by BLI (Fig. 7) to ascertain whether these mutations would confer cross-reactivity to other B41-specific glycan hole antibodies. All four antibodies bound B41 as expected, with binding quickly reaching saturation levels with no detectable off-rates. 16D did, however, exhibit a slower binding on-rate than others, which also shows an order-of-

magnitude-lower neutralization against B41 pseudovirus (Fig. 1D). In contrast, none of the four antibodies bound to any of the four trimer variants tested, namely, BG505_wt, BG505_293S_deglyco, BG505_mut123, or BG505 mut123_N241. In addition to being derived from distinct antibody lineages, the sequence alignment of the CDRH3 region shows that the sequence and length varies between rabbit nAbs, which likely results in different molecular interactions at the epitope-paratope interface from those observed for 13B. This result further emphasizes the strain-specific nature of the mAb responses and the different ways that antibodies can recognize the glycan hole epitope.

DISCUSSION

Our structural studies show that immunization with the clade B trimer B41 SOSIP resulted in two epitope regions targeted by all isolated antibodies, namely, autologous glycan hole-targeting antibodies as well as nonneutralizing base-binding antibodies. Serum analyses in previous studies have shown that the glycan hole epitope region commonly elicited autologous nAb responses in B41 and BG505 SOSIP immunizations (13, 14, 18). Furthermore, polyclonal epitope analysis in rabbits (18) and nonhuman primates (35) of BG505 SOSIP trimer immunizations demonstrated that glycan hole antibodies are frequently elicited, making it an important epitope to understand so that it could potentially be exploited for cross-reactive immunization strategies.

Here, we endeavored to elucidate the basis for the lack of cross-reactivity of the glycan hole nAbs that were elicited by B41 and BG505 SOSIP immunogens. Despite isolating antibodies that bound to B41 and BG505 SOSIP baits, none of these were neutralizing, and therefore, they likely target the irrelevant base epitope. Of the remaining isolated antibodies that were successfully cloned, binding was confined to only B41. While this is certainly not an exhaustive set of antibodies, our experiments yielded a representative set of antibodies to further characterize and probe for cross-reactive potential.

A comparison of the low-resolution NS-EM reconstructions of BG505 trimers in complex with BG505 nAb 11A and B41 trimers in complex with B41 nAbs 13B and 49A revealed highly overlapping epitopes and angles of approach. While the introduction of glycans at positions 230 and 289 in BG505 completely abolished neutralizing activity for 10A, 11A, and 11B (13), neutralization for the B41 nAbs was abolished for N289 but was only partially reduced by ~20% for N230 when introduced into B41. Interestingly, when the N230 and N289 knock-in viruses were produced in the presence of kifunensine, N230 neutralization was increased and N289 neutralization was even restored to some degree. Growth of virus in kifunensine results in more homogeneous, oligomannose glycans and may cause structural changes that alter the accessibility of the glycan-hole epitopes. This suggests that complex glycans at N289 are a particularly strong barrier to the glycan hole epitope. Removal of glycan N241 in B41 reduced the neutralizing activity of the B41 nAbs, suggesting a potential direct role in binding. Our structural studies showed that 13B is in close proximity of the N241 glycan, although we did not observe any specific interactions, despite an ~70-fold reduction in neutralization when this glycan was removed. These data suggest that the absence of the N241 glycan has an indirect effect, for example, by altering glycan processing of adjacent glycans. Altogether, these observations suggest that the B41 nAbs are impacted by more heterogeneous complex glycans, particularly when N289 is introduced. Similar to BG505, the N289 glycan knocks out neutralization of B41 glycan hole nAbs. B41 is, however, less impacted by the N230 glycan. Because the glycans only reduce binding and there are no specific contacts with any glycans, the underlying amino acids that comprise the epitope must be responsible for the strain specificity.

The NS-EM and ELISA competition assay demonstrated that all antibodies bind to the 230/289 glycan hole epitope in a similar fashion, suggesting subtle differences at the amino acid level. To further investigate these details, we tested the binding of B41-specific nAbs to BG505 with B41 mutants that were based on the amino acid contacts that we observed in our cryoEM structure of B41 SOSIP bound to 13B. Among all of the different B41 nAbs tested, only 13B recovered partial binding to BG505-

mut123. This finding is not that surprising given that the sequences of CDRH3 in the B41-specific nAbs were relatively diverse. These data, and the lack of any neutralization in the viruses lacking the N289 glycan in the 117-virus panel, demonstrate the very narrow strain specificity of these mAbs (Fig. S4).

We attempted to reveal the structural basis for the lack of cross-reactivity nAbs that target a similar epitope region in the BG505 and B41 immunogens. While we analyzed too few animals to categorically state that BG505 and B41 responses cannot overlap, our results demonstrate that it may be infrequent. Using the cryoEM structure of the B41 SOSIP trimer in complex with nAb 13B, we determined that B41- and BG505-specific nAbs target amino acids that differ between the strains. While we could recover partial binding by substituting residues, broadening antibody responses to the N289 glycan hole site is likely to remain a challenging prospect. While we could envision broadening B41-specific responses using one of our intermediate mutated trimers (e.g., BG505_mut123_N241) as a boost immunogen to bridge toward BG505 cross-reactivity, this boost would likely be specific to a single antibody lineage, namely, 13B, which was only present in one rabbit. Thus, even with the increased knowledge gained from all of the analyses here, HIV immunogen design for broader antibody responses at glycan hole sites remains challenging.

MATERIALS AND METHODS

Immunizations. Immunization details are summarized in Fig. 1A. Animals 5713 and 5716 received 30 μg B41 SOSIP trimer alone. Animal 5746 received a BG505 SOSIP and B41 SOSIP cocktail (1 to 1 ratio), with total dose of 10 μg. Animal 5749 received a BG505 SOSIP and B41 SOSIP cocktail (1 to 1 ratio), with a dose of 30 μg each time, respectively. The immunization of animals 5745 and 5748 were described in a previous study (14). Immunogens were formulated with 75 units of Iscomatrix, a saponin-based adjuvant obtained from CSL Ltd. (Parkville, Victoria, Australia) via the International AIDS Vaccine Initiative. Immunization was approved and carried out in accordance with protocols provided to the Institutional Animal Care and Use Committee (IACUC) at Covance Research Products (CRP) Inc. (Denver, PA), under approval number C0014-15 (14).

Neutralization assays and pseudovirus production. Single-round infectious HIV-1 Env pseudoviruses were produced as described previously (Seaman et al., 2010). Briefly, plasmids encoding Env were cotransfected with an Env-deficient backbone plasmid (pSG3DENV) using Fugene 6 (Promega). Virus-containing supernatants were harvested at 48 h posttransfection, stored at −80°C, and then titrated on TZM-bl target cells to determine the dilution appropriate for the neutralization assays. Pseudovirus neutralization assays using TZM-bl target cells were carried out as previously described (22). Prior to evaluation, mAbs were purified as described below and passed through a 0.22-μM filter. Plasma samples were heat inactivated at 50°C for 30 minutes and then passed through a 0.22-μM filter. mAbs and/or plasma were then serially diluted in a 96-well plate and incubated with virus for 1 h before adding to TZM-bl target cells. After 48 hours, the relative light units (RLUs) for each well were measured and neutralization calculated as the decrease in RLU relative to virus-only control wells. ID_{50}/IC_{50} values are reported as the reciprocal dilution/antibody concentration that resulted in 50% virus neutralization after fitting the curve of log concentration (plasma/mAb) versus percent neutralization in Prism. For kifunensine (kif)-grown viruses, 25 mM kifunensine was added to 293T cells on the day of transfection.

Antibody isolation. Cryopreserved peripheral blood mononuclear cells (PBMCs) were thawed, resuspended in 10 ml of Roswell Park Memorial Institute (RPMI) medium with 10% fetal calf serum (FCS), and collected by centrifugation at 600 × *g* for 5 min. Cells were washed with phosphate-buffered saline (PBS), resuspended in 10 ml of PBS, and collected by a second centrifugation step. Cells were resuspended in 100 μl of FACS wash buffer (FWB) (2% FCS/PBS) with anti-rabbit IgG fluorescein isothiocyanate (FITC) (1:1000), 1 μl of a streptavidin-phycoerythrin (PE) tetramer of biotinylated BG505 SOSIP, and 1 μl of a streptavidin-allophycocyanin (APC) tetramer of biotinylated B41 SOSIP. After 1 h on ice, cells were washed once with 10 ml of PBS, collected by centrifugation, and resuspended in 500 μl of FWB for sorting on a BD fluorescence-activated cell sorter (FACS) Aria III instrument. IgG^+ lymphocytes that stained positive for either/both BG505 or B41 tetramers were collected at 1 cell per well into Superscript III reverse transcriptase lysis buffer (Invitrogen) as previously described and immediately stored at −80°C.

cDNA was generated using Superscript III reverse transcription (Invitrogen) as previously described (23). First-round PCR products were produced using 2.5 μl of cDNA and Hotstart *Taq* master mix (Qiagen) for 50 cycles using the first-round primers as reported previously (13). Subsequently, 2.5 μl of first-round PCR product was used as the template for the second round using the second-round primers as reported previously (13). PCR products were sequenced and then analyzed using the IMGT Vquest tool. MAb lineages were identified as those with highly similar CDRH3 loop sequences. Heavy chain- and light chain-variable regions were then amplified by PCR with primers (13) containing homology arms specific for the expression vector. PCR products and vector were ligated using high-fidelity assembly mix (New England BioLabs [NEB]) into expression plasmids adapted from the pFUSE-rIgG-Fc and pFUSE2-CLIg-rK2 vectors (Invivogen). Human and rabbit Abs were transiently expressed with the FreeStyle 293 Expression

System (Invitrogen). Abs were purified using affinity chromatography (protein A Sepharose fast flow; GE Healthcare).

Two non-nAbs (45A and 48A) were isolated in parallel from studies described previously (14) and used as controls. The negative-control mAb, named Hybrid, was made from the heavy chain of R56 and light chain of R20 (PDB 4JO3) used in a previous study (13).

Competition ELISAs. The 96-well plates were coated overnight at 4°C with mouse anti-Avi-tag antibody (Genscript) at 2 μg/ml in PBS. Plates were washed 4 times with PBS and 0.05% (vol/vol) Tween and blocked with 3% (wt/vol) bovine serum albumin (BSA) in PBS for 1 h. Concurrently, 5-fold serial dilutions from 50 μg/ml of rabbit or human mAbs were preincubated with 1 μg/ml of purified Avi-tagged SOSIP protein for 1 h. The mAb-SOSIP mixture was then transferred to the ELISA plate and incubated for 1 h. Plates were washed four times and incubated with 0.5 μg/ml of biotinylated mAb for 1 h and were washed again; binding was detected with streptavidin-alkaline phosphatase (Jackson Immunoresearch) at 1:1000 for 1 h. MAbs were biotinylated using the *N*-hydroxysuccinimide (NHS)-micro biotinylation kit (Pierce).

Mutations, protein expression, and purification. To produce mutant viruses, the parental Env-encoding plasmid was altered by site-directed mutagenesis using the QuikChange site-directed mutagenesis kit (Agilent) according to the manufacturer's instructions. Sanger sequencing was performed to verify that each plasmid encoded the desired mutation. Mutant pseudoviruses were then produced by cotransfection with pSG3DENV, as described above. Mutations in BG505 SOSIP were generated by Agilent QuikChange Lightning multisite-directed mutagenesis kit and confirmed by Genewiz sequencing.

All untagged B41 SOSIP and BG505 SOSIP were expressed using HEK 293F cells for 6 days and then purified on a 2G12 IgG cross-linked Sepharose column. The proteins were eluted by 3 M $MgCl_2$ (pH 7.2) buffer and then further purified over a HiLoad 16/600 Superdex 200 pg column in 20 mM Tris (pH 7.4) plus 150 mM NaCl (1× Tris-buffered saline [TBS]) buffer.

All C-term His_6-tagged B41 SOSIP and BG505 SOSIP mutants were expressed using HEK 293F cells for 6 days and then purified on a 2G12 IgG cross-linked Sepharose column. The proteins were eluted with 3 M $MgCl_2$ (pH 7.2) + 250 mM L-arginine buffer and then further purified over a HiLoad 16/600 Superdex 200-pg column in 20 mM Tris (pH 7.4) with 150 mM NaCl + 250 mM L-arginine buffer. Notably, 250 mM L-arginine was added to prevent aggregation for Env trimers with added C-term His_6-tags.

BG505 with high mannose glycans was expressed using HEK 293S cells for 6 days and then purified on a 2G12 IgG cross-linked Sepharose column. The trimers were eluted by 3 M $MgCl_2$ (pH 7.2) + 250 mM L-arginine buffer and then further purified over a HiLoad 16/600 Superdex 200 pg column in 20 mM Tris (pH 7.4) with 150 mM NaCl + 250 mM L-arginine buffer. Purified BG505 was cleaved by an EndoH enzyme overnight to remove glycans and then purified over a HiLoad 16/600 Superdex 200-pg column in 20 mM Tris (pH 7.4) with 150 mM NaCl + 250 mM L-arginine buffer.

Fabs from rabbits were expressed in 293F cells for 6 days and then affinity purified using a CaptureSelect CH1-XL prepacked 1-ml column (ThermoFisher).

Biolayer interferometry. His_6-tagged B41 SOSIP and His_6-tagged BG505 SOSIP variants at 0.05 mg/ml were loaded onto Ni-nitrilotriacetic acid (NTA) biosensors and dipped into 1 μM (300 μl) of rabbit Fab using an Octet Red96 instrument (ForteBio). After loading for 180 s, association was measured for 180 s, followed by dissociation for 600 s in 1× kinetics buffer (phosphate-buffered saline [pH 7.2], 0.01% [wt/vol] BSA, and 0.002% [vol/vol] Tween 20). A baseline containing no trimer sample, but the same concentration of Fab in 1× kinetics buffer, was subtracted from each data set, and curves were aligned on the *y* axis using the baseline step. Baseline subtraction minimized the influence of nonspecific binding of Fab to the sensor tip.

Negative-stain EM sample preparation, data collection, and processing. All trimer-Fab complexes were generated by incubating 10× molar Fab with B41 SOSIP or BG505 SOSIP mutants overnight at room temperature. Grid preparation, image processing, and raw data analysis followed a similar protocol described previously (24). Briefly, samples were diluted with 1× TBS to 0.01 mg/ml right before putting on grids. Three microliters of sample was then applied to a 400 mesh carbon-coated Cu grid and then stained with 2% (wt/vol) uranyl formate for 45 to 60 s. Grids were blotted using blotting paper until completely dry. All grids were imaged on a 120 keV FEI Tecnai Spirit electron microscope using a nominal magnification of ×52,000, resulting in 2.05 Å/px. Micrographs were collected with a TVIPS TemCam-F416 (4k x 4k) camera using the Leginon interface (25) with a defocus of 1.5 μm.

Particles were selected using Appion DoGPicker (26) and extracted with Relion v2.1.(27) Extracted particles were imported to cryosparc v2.8.0 (28). Particles were then classified in 2D into 50 classes. Classes not containing features of trimers were removed, and the remaining particles were used for three-dimensional (3D) refinement. The NS-EM 3D reconstructions have been deposited to the Electron Microscopy Data Bank under numbers B41-45A (EMD-20882), B41-48A (EMD-20737), and B41-49A (EMD-20738).

CryoEM sample preparation, data collection, and processing. B41 SOSIP trimers were complexed with 6× molar excess of 13B Fab overnight at room temperature and then purified by a HiLoad 16/600 Superdex 200-pg column. The eluted samples were concentrated to 5 mg/ml and applied to previously plasma-cleaned Protochips C-flat 2/2 400 mesh Cu grids, which were blotted once for 5 s with blot force 0 after a wait time of 10 s. Blotted grids were plunge frozen into nitrogen-cooled liquid ethane using a Vitrobot Mark IV device (ThermoFisher).

Data were collected on a Talos Arctica operating at 200 kV coupled with a K2 Summit direct electron detector at a nominal magnification of ×36,000, resulting in 1.15-Å pixel size. Dose was calculated to be 5.67 e-/pix/s. A total of 47 frames were collected per movie, with 250-ms exposure time each, resulting

in a total dose of ~50.4 electrons $Å^{-2}$. Micrographs were collected with the automated Leginon interface (25) using a defocus range from 0.8 to 2 μm.

Movies were aligned and dose-weighted using MotionCor2 (29) (see Fig. S1A in the supplemental material). Data were then processed with Cryosparc v2 (28) (Fig. S1B). A total of 1,721 micrographs were used. Particles were then classified in 2D by 50 classes, and classes not containing features of trimers were removed, resulting in particle images that were retained for further processing.

The final refinement included 145,000 particles, and C3 symmetry was imposed. The resolution of the final map was calculated to ~3.9 Å at a Fourier shell correlation (FSC) cutoff at 0.143. The EM reconstructions have been deposited to the Electron Microscopy Data Bank (EMD-20642).

Modeling and refinement of cryoEM structures. Initial homology models of B41 (gp120 and gp41) were generated using the crystal structure of B41 (PDB 6MCO). An initial model of the Fv region of 13B was generated using the Rosetta antibody protocol available on the ROSIE server (20). Individual chains were fit into the 3.9-Å cryoEM map using UCSF Chimera (21). Glycans were built with Coot (30). Sugar molecules with disordered or no density were removed. The structure was then refined using Rosetta real space refinement (31), requesting an output of 319 refined structural models. The top scoring structure was chosen after evaluation with MolProbity (32) and EMRinger (33) and after manual inspection. The model was iteratively refined using Rosetta real space refinement and improved by manual inspection using Coot. CryoEM data collection and refinement statistics are summarized in Table S1 in the supplemental material. Structural figures were made in UCSF Chimera. Regions with relatively poor density in the model were removed. The model has been deposited to the Protein Data Bank (PDB 6U59).

SUPPLEMENTAL MATERIAL

Supplemental material is available online only.

SUPPLEMENTAL FILE 1, PDF file, 0.7 MB.

ACKNOWLEDGMENTS

The research was supported by NIH grants UM1AI100663 and UM1AI144462 (I.A.W., A.B.W., and D.R.B.) and P01 AI110657 (I.A.W., A.B.W., and R.W.S.); Bill and Melinda Gates Foundation grants OPP1115782 (A.B.W.) and OPP1132237 (R.W.S.); and amfAR grant 109514-61-RKVA (M.J.V.G.). R.W.S. is a recipient of a Vici grant from the Netherlands Organization for Scientific Research (NWO). C.A.C. was supported by NIH F31 Ruth L. Kirschstein Predoctoral Award AI131873 and by the Achievement Rewards College Scientists Foundation.

We are grateful to Bill Anderson for expert microscopy assistance; to Lauren Holden, Aleks Antanasijevic, and Julianna Han for manuscript proofreading and editing; and to Leigh Sewall and Jeffrey Copps for expert biochemical and technical assistance.

REFERENCES

1. Moore PL, Crooks ET, Porter L, Zhu P, Cayanan CS, Grise H, Corcoran P, Zwick MB, Franti M, Morris L, Roux KH, Burton DR, Binley JM. 2006. Nature of nonfunctional envelope proteins on the surface of human immunodeficiency virus type 1. J Virol 80:2515–2528. https://doi.org/10.1128/JVI.80.5.2515-2528.2006.
2. Poignard P, Moulard M, Golez E, Vivona V, Franti M, Venturini S, Wang M, Parren P, Burton DR. 2003. Heterogeneity of envelope molecules expressed on primary human immunodeficiency virus type 1 particles as probed by the binding of neutralizing and nonneutralizing antibodies. J Virol 77:353–365. https://doi.org/10.1128/jvi.77.1.353-365.2003.
3. Falkowska E, Le KM, Ramos A, Doores KJ, Lee JH, Blattner C, Ramirez A, Derking R, van Gils MJ, Liang C-H, McBride R, von Bredow B, Shivatare SS, Wu C-Y, Chan-Hui P-Y, Liu Y, Feizi T, Zwick MB, Koff WC, Seaman MS, Swiderek K, Moore JP, Evans D, Paulson JC, Wong C-H, Ward AB, Wilson IA, Sanders RW, Poignard P, Burton DR. 2014. Broadly neutralizing HIV antibodies define a glycan-dependent epitope on the prefusion conformation of gp41 on cleaved envelope trimers. Immunity 40:657–668. https://doi.org/10.1016/j.immuni.2014.04.009.
4. Blattner C, Lee JH, Sliepen K, Derking R, Falkowska E, de la Peña AT, Cupo A, Julien J-P, van Gils M, Lee PS, Peng W, Paulson JC, Poignard P, Burton DR, Moore JP, Sanders RW, Wilson IA, Ward AB. 2014. Structural delineation of a quaternary, cleavage-dependent epitope at the gp41-gp120 interface on intact HIV-1 Env trimers. Immunity 40:669–680. https://doi.org/10.1016/j.immuni.2014.04.008.
5. Burton DR, Mascola JR. 2015. Antibody responses to envelope glycoproteins in HIV-1 infection. Nat Immunol 16:571–576. https://doi.org/10.1038/ni.3158.
6. Eroshkin AM, LeBlanc A, Weekes D, Post K, Li Z, Rajput A, Butera ST, Burton DR, Godzik A. 2014. bNAber: database of broadly neutralizing HIV antibodies. Nucleic Acids Res 42:D1133–D1139. https://doi.org/10.1093/nar/gkt1083.
7. Burton DR. 2019. Advancing an HIV vaccine; advancing vaccinology. Nat Rev Immunol 19:77–78. https://doi.org/10.1038/s41577-018-0103-6.
8. Burton DR, Hangartner L. 2016. Broadly neutralizing antibodies to HIV and their role in vaccine design. Annu Rev Immunol 34:635–659. https://doi.org/10.1146/annurev-immunol-041015-055515.
9. Torrents de la Peña A, de Taeye SW, Sliepen K, LaBranche CC, Burger JA, Schermer EE, Montefiori DC, Moore JP, Klasse PJ, Sanders RW. 2018. Immunogenicity in rabbits of HIV-1 SOSIP trimers from clades A, B, and C, given individually, sequentially, or in combination. J Virol 92:e01957-17. https://doi.org/10.1128/JVI.01957-17.
10. Shaffer JS, Moore PL, Kardar M, Chakraborty AK. 2016. Optimal immunization cocktails can promote induction of broadly neutralizing Abs against highly mutable pathogens. Proc Natl Acad Sci U S A 113:E7039–E7048. https://doi.org/10.1073/pnas.1614940113.
11. Schülke N, Vesanen MS, Sanders RW, Zhu P, Lu M, Anselma DJ, Villa AR, Parren P, Binley JM, Roux KH, Maddon PJ, Moore JP, Olson WC. 2002. Oligomeric and conformational properties of a proteolytically mature, disulfide-stabilized human immunodeficiency virus type 1 gp140 envelope glycoprotein. J Virol 76:7760–7776. https://doi.org/10.1128/jvi.76.15.7760-7776.2002.
12. Sanders RW, Vesanen M, Schuelke N, Master A, Schiffner L, Kalyanaraman R, Paluch M, Berkhout B, Maddon PJ, Olson WC, Lu M, Moore JP. 2002. Stabilization of the soluble, cleaved, trimeric form of the envelope

glycoprotein complex of human immunodeficiency virus type 1. J Virol 76:8875–8889. https://doi.org/10.1128/jvi.76.17.8875-8889.2002.
13. McCoy LE, van Gils MJ, Ozorowski G, Messmer T, Briney B, Voss JE, Kulp DW, Macauley MS, Sok D, Pauthner M, Menis S, Cottrell CA, Torres JL, Hsueh J, Schief WR, Wilson IA, Ward AB, Sanders RW, Burton DR. 2016. Holes in the glycan shield of the native HIV envelope are a target of trimer-elicited neutralizing antibodies. Cell Rep 16:2327–2338. https://doi.org/10.1016/j.celrep.2016.07.074.
14. Klasse PJ, LaBranche CC, Ketas TJ, Ozorowski G, Cupo A, Pugach P, Ringe RP, Golabek M, van Gils MJ, Guttman M, Lee KK, Wilson IA, Butera ST, Ward AB, Montefiori DC, Sanders RW, Moore JP. 2016. Sequential and simultaneous immunization of rabbits with HIV-1 envelope glycoprotein SOSIP.664 trimers from clades A, B and C. PLoS Pathog 12:e1005864. https://doi.org/10.1371/journal.ppat.1005864.
15. Foley BLT, Apetrei C, Hahn B, Mizrachi I, Mullins J, Rambaut A, Wolinsky S, Korber B (ed). 2018. HIV sequence compendium 2018. Theoretical Biology and Biophysics Group, Los Alamos National Laboratory, Los Alamos, NM.
16. Wagh K, Kreider EF, Li Y, Barbian HJ, Learn GH, Giorgi E, Hraber PT, Decker TG, Smith AG, Gondim MV, Gillis L, Wandzilak J, Chuang G-Y, Rawi R, Cai F, Pellegrino P, Williams I, Overbaugh J, Gao F, Kwong PD, Haynes BF, Shaw GM, Borrow P, Seaman MS, Hahn BH, Korber B. 2018. Completeness of HIV-1 envelope glycan shield at transmission determines neutralization breadth. Cell Rep 25:893–908.e7. https://doi.org/10.1016/j.celrep.2018.09.087.
17. Pugach P, Ozorowski G, Cupo A, Ringe R, Yasmeen A, de Val N, Derking R, Kim HJ, Korzun J, Golabek M, de los Reyes K, Ketas TJ, Julien J-P, Burton DR, Wilson IA, Sanders RW, Klasse PJ, Ward AB, Moore JP. 2015. A native-like SOSIP.664 trimer based on an HIV-1 subtype B env gene. J Virol 89:3380–3395. https://doi.org/10.1128/JVI.03473-14.
18. Bianchi M, Turner HL, Nogal B, Cottrell CA, Oyen D, Pauthner M, Bastidas R, Nedellec R, McCoy LE, Wilson IA, Burton DR, Ward AB, Hangartner L. 2018. Electron-microscopy-based epitope mapping defines specificities of polyclonal antibodies elicited during HIV-1 BG505 envelope trimer immunization. Immunity 49:288–300.e8. https://doi.org/10.1016/j.immuni.2018.07.009.
19. Klasse PJ, Ketas TJ, Cottrell CA, Ozorowski G, Debnath G, Camara D, Francomano E, Pugach P, Ringe RP, LaBranche CC, van Gils MJ, Bricault CA, Barouch DH, Crotty S, Silvestri G, Kasturi S, Pulendran B, Wilson IA, Montefiori DC, Sanders RW, Ward AB, Moore JP. 2018. Epitopes for neutralizing antibodies induced by HIV-1 envelope glycoprotein BG505 SOSIP trimers in rabbits and macaques. PLoS Pathog 14:e1006913. https://doi.org/10.1371/journal.ppat.1006913.
20. Lyskov S, Chou F-C, Conchúir SÓ, Der BS, Drew K, Kuroda D, Xu J, Weitzner BD, Renfrew PD, Sripakdeevong P, Borgo B, Havranek JJ, Kuhlman B, Kortemme T, Bonneau R, Gray JJ, Das R. 2013. Serverification of molecular modeling applications: the Rosetta Online Server That Includes Everyone (ROSIE). PLoS One 8:e63906. https://doi.org/10.1371/journal.pone.0063906.
21. Pettersen EF, Goddard TD, Huang CC, Couch GS, Greenblatt DM, Meng EC, Ferrin TE. 2004. UCSF Chimera—a visualization system for exploratory research and analysis. J Comput Chem 25:1605–1612. https://doi.org/10.1002/jcc.20084.
22. Li M, Gao F, Mascola JR, Stamatatos L, Polonis VR, Koutsoukos M, Voss G, Goepfert P, Gilbert P, Greene KM, Bilska M, Kothe DL, Salazar-Gonzalez JF, Wei X, Decker JM, Hahn BH, Montefiori DC. 2005. Human immunodeficiency virus type 1 env clones from acute and early subtype B infections for standardized assessments of vaccine-elicited neutralizing antibodies. J Virol 79:10108–10125. https://doi.org/10.1128/JVI.79.16.10108-10125.2005.
23. Sok D, van Gils MJ, Pauthner M, Julien JP, Saye-Francisco KL, Hsueh J, Briney B, Lee JH, Le KM, Lee PS, Hua Y, Seaman MS, Moore JP, Ward AB, Wilson IA, Sanders RW, Burton DR. 2014. Recombinant HIV envelope trimer selects for quaternary-dependent antibodies targeting the trimer apex. Proc Natl Acad Sci U S A 111:17624–17629. https://doi.org/10.1073/pnas.1415789111.
24. Lei L, Yang YR, Tran K, Wang Y, Chiang C-I, Ozorowski G, Xiao Y, Ward AB, Wyatt RT, Li Y. 2019. The HIV-1 envelope glycoprotein C3/V4 region defines a prevalent neutralization epitope following immunization. Cell Rep 27:586–598.e6. https://doi.org/10.1016/j.celrep.2019.03.039.
25. Carragher B, Kisseberth N, Kriegman D, Milligan RA, Potter CS, Pulokas J, Reilein A. 2000. Leginon: an automated system for acquisition of images from vitreous ice specimens. J Struct Biol 132:33–45. https://doi.org/10.1006/jsbi.2000.4314.
26. Lander GC, Stagg SM, Voss NR, Cheng A, Fellmann D, Pulokas J, Yoshioka C, Irving C, Mulder A, Lau P-W, Lyumkis D, Potter CS, Carragher B. 2009. Appion: an integrated, database-driven pipeline to facilitate EM image processing. J Struct Biol 166:95–102. https://doi.org/10.1016/j.jsb.2009.01.002.
27. Zhang K. 2016. Gctf: real-time CTF determination and correction. J Struct Biol 193:1–12. https://doi.org/10.1016/j.jsb.2015.11.003.
28. Punjani A, Rubinstein JL, Fleet DJ, Brubaker MA. 2017. cryoSPARC: algorithms for rapid unsupervised cryo-EM structure determination. Nat Methods 14:290–296. https://doi.org/10.1038/nmeth.4169.
29. Zheng SQ, Palovcak E, Armache J-P, Verba KA, Cheng Y, Agard DA. 2017. MotionCor2: anisotropic correction of beam-induced motion for improved cryo-electron microscopy. Nat Methods 14:331–332. https://doi.org/10.1038/nmeth.4193.
30. Emsley P, Cowtan K. 2004. Coot: model-building tools for molecular graphics. Acta Crystallogr D Biol Crystallogr 60:2126–2132. https://doi.org/10.1107/S0907444904019158.
31. Wang RY-R, Song Y, Barad BA, Cheng Y, Fraser JS, DiMaio F. 2016. Automated structure refinement of macromolecular assemblies from cryo-EM maps using Rosetta. Elife 5:e17219. https://doi.org/10.7554/eLife.17219.
32. Chen VB, Arendall WB, Headd JJ, Keedy DA, Immormino RM, Kapral GJ, Murray LW, Richardson JS, Richardson DC. 2010. MolProbity: all-atom structure validation for macromolecular crystallography. Acta Crystallogr D Biol Crystallogr 66:12–21. https://doi.org/10.1107/S0907444909042073.
33. Barad BA, Echols N, Wang R-R, Cheng Y, DiMaio F, Adams PD, Fraser JS. 2015. EMRinger: side chain–directed model and map validation for 3D cryo-electron microscopy. Nat Methods 12:943–946. https://doi.org/10.1038/nmeth.3541.
34. Larsson A. 2014. AliView: a fast and lightweight alignment viewer and editor for large datasets. Bioinformatics 30:3276–3278. https://doi.org/10.1093/bioinformatics/btu531.
35. Nogal B, Bianchi M, Cottrell CA, Kirchdoerfer RN, Sewall LM, Turner HL, Zhao F, Sok D, Burton DR, Hangartner L, Ward AB. 2019. Mapping polyclonal antibody responses in non-human primates vaccinated with HIV Env trimer subunit vaccines. bioRxiv https://doi.org/10.1101/833715.